Investigating frictional properties of the Longitudinal Valley fault from dynamic modeling of pre- and postseismic slip associated with the 2003, Mw 6.8 Chengkung earthquake.

Shu-Hao Chang[1], Marion Thomas[1], Jian-Cheng Lee[2], Sylvain Barbot[1] and Jean-Philippe Avouac[1]

[1]Geological and Planetary Sciences, California Institute of Technology

[2]Institute of Earth Sciences, Academia Sinica

1. Background

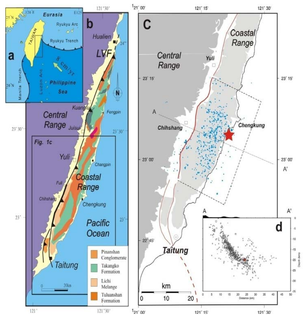

Figure 1. (a) Plate-tectonic setting of Taiwan. (b) General geology of the Coastal Range. The Coastal Range is thrust onto the Longitudinal Valley and the Central Range along the active Longitudinal Valley fault (LVF) (heavy line with triangles pointing in dip direction). (c) Seismicity map of main shock (star) and aftershocks (dots) of the 2003 Mw 6.8 Chengkung earthquake. (d) Cross section of the distribution of the 2003 earthquake sequence. (Lee et al. 2006)

The active Chihshang fault shows a vigorous creep at the boundary between the Eurasian and the Philippine Sea plates along the Longitudinal Valley in eastern Taiwan. However, it has also produced large earthquakes at mid-crustal depth such as the 2003 Mw 6.8 Chengkung earthquake (Fig. 1). As a result, it appears that the fault behaviors varied through time. Furthermore, the creep rate measured by creep meters at the surface level during the interseismic period shows strong seasonal fluctuations [Lee et al., 2003], which seemingly correlated with precipitation. The Chengkung earthquake nucleated at about 20 km deep and ruptured the entire Chihshang fault but with a very small amount of coseismic slip near the surface [Lee et al., 2006; Wu et al., 2006; Ching et al., 2007; Cheng et al., 2009]. The accumulated seismic energy at the shallow level soon was relaxed by a sudden increase of creep after the main shock that decayed with time during the post-seismic period. These observations of interseismic creep and rapid post-seismic slip suggest that the fault slip obeys a rate-strengthening friction law near surface, during both interseismic and coseismic periods. Hence the physical or mechanical properties of the fault zone near the surface level likely play a crucial role on the fault slip behaviors, which reflected on the dry season locked and on the impediment of coseismic slip propagation to the surface.

2. Continuous GPS data

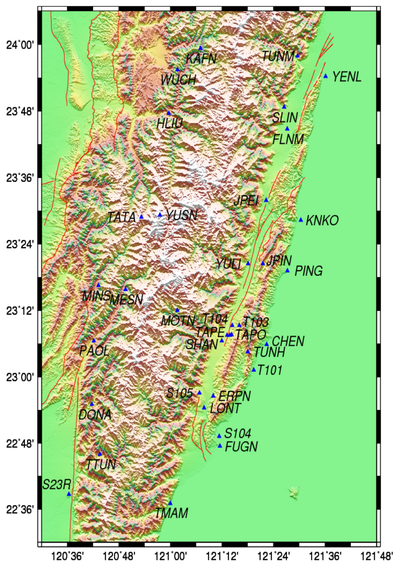

Figure 3. The continuous GPS record at site CHEN. The north component is showed by green dots and the east component is showed by red dots. The blue dots show the deformation in vertical. The black line indicates the interpolations of the observed data. The vertical red dash line means the day that the Chengkung earthquake occurred and the vertical axis indicates the displacement in directions by millimeter. Significant after-slips followed the 10 December (*Mw* = 6.8) Chengkung earthquake, until mid-2004 that are similar to the other continuous GPS data near the Chihshang Fault.

There are more than 60 continuous Global Positioning System (GPS) sites in this area. 20 of them are close to Chihshang fault and are well recorded from 1999 to now. In this study, we intend to use these 20 continuous GPS stations near the Chihshang fault, which are operated by several different institutions, including Institute of Earth Sciences, Academia Sinica, National Taiwan University, Ministry of the interior, and Central Weather Bureau (Fig. 2). The continuous GPS data compactly recorded not only the interseismic surface deformation but particularly also that associated with the Chengkung earthquake (Fig. 3). In this study, we intend to adopt the GPS data to invert the afterslip on the Chihshang Fault and then estimate the friction parameters on the same fault plane.

Figure 2. General morphologic features of the active Chihshang fault and location of continuous GPS sites.

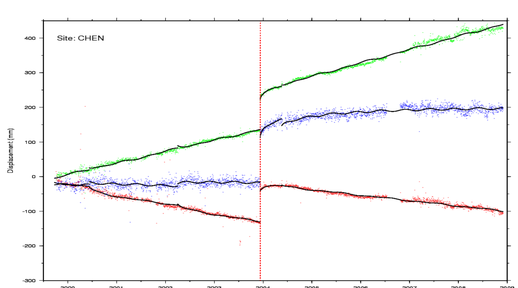

3. Theory and Method

We follow Perfettini and Avouac (2007) by assuming that the frictional behaviour of the afterslips of the Chihshang fault obeys a pure velocity-strengthening rheology:

$$\tau = \sigma\mu^{*} + a\sigma\ln\left(\frac{V}{V^{*}}\right)$$

where τ and σ are the shear and effective normal stresses on the fault plane; μ* is the friction coefficient under reference slip rate V* ; a is an empirical constant and V is fault slip rate. The state of stress on a fault plane evolves as the combination of initial stress, stress change due to creep and stress change due to earthquake. As a result, for a fault plane with n subfaults, stress balance on a subfault i at time t requires

$$\tau(i,t) = \tau_0(i) + \Delta\tau\_creep(i,t) + \Delta\tau\_eq(i) \text{ and}$$

$$\sigma(i,t) = \sigma_0(i) + \Delta\sigma\_creep(i,t) + \Delta\sigma\_eq(i) - \Delta P\_f(i,t),$$

where $\tau_0(i)$ and $\sigma_0(i) - \Delta P\_f(i, t = 0)$ are the initial shear and effective normal stresses; Δτ_creep(i , t) and Δσ_creep(i , t) are changes in shear and effective normal stresses by evolution of fault slip in the creeping zone; Δτ_eq(i) and Δσ_eq(i) are shear and effective normal stresses induced by earthquakes; P_f (i , t) is pore pressure change in the fault zone due to fluctuation of groundwater level. Combining these eqs. and replacing V* with V_o, we obtain that

$$V(i,t) = V_0(i)\exp\left[(\Delta CFF(i,t) + CFF_0)/a(i)\sigma(i,t)\right],$$

where V(i , t) is the slip rate of subfault i at time t, and $\Delta CFF(i,t) = \Delta\tau(i,t) - \mu_0(i)\Delta\sigma(i,t)$ is the Coulomb stress change with $\mu_0(i)$ denoting the friction coefficient at long-term loading velocity V_0 (i), Δτ(i , t) and Δσ(i , t) denoting the changes in shear and effective normal stresses of subfault i at time t with respect to their initial values. $CFF_0 = \tau_0(i) - \mu_0(i)\sigma_0(i)$ is the initial stress. We solve this eq. with an implicit finite-difference method and the optimal values of a, μ_o, V_0 and rake of each subfault are determined by employing the public neighbourhood algorithm driver of Sambridge M. (1999) to minimize an objective function, which is defined as s/r, with r denoting the correlation coefficient between the observed and calculated creep series, and s denoting the root mean-squared misfit between the observed and the modelled slip. We set up the searching range from 0.0005 to 0.02 for parameter a, from 0.1 to 0.85 for the friction coefficient μ_0 and from 1.0 to 100 mm/yr for the slip velocity V_0.

4. Numerical model

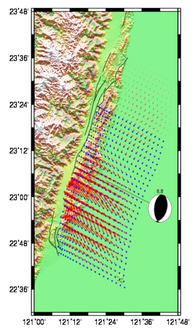

We used a 27 by 20 three dimension curve coseismic rupture model to evaluate the coseismic stress changes in the creep zone due to the Chengkung earthquake. The asperity of coseismic slips is in the south of the focus. The same grid points are used as the afterslip fault grid points.

Figure 4. Numerical model geometry. The red vectors are the coseismic slips of the Chengkung earthquake derived by PCAIM from Thomas et al. (2010). The blue dots indicate the center of each subfault of the afterslip fault plane. The focal mechanism shows a thrust slip of Chengkung earthquake.

Acknowledgments

We are very grateful to the Gordon and Betty Moore Foundation for their support on this poster. Some of the figures in this poster were made using Generic Mapping Tools (GMT).

5. Primarily results

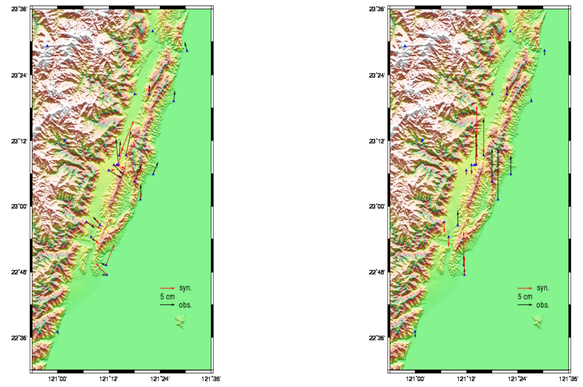

From the surface displacements at the last day of the evolution, we can see that the postseismic deformations could be generated by a dynamic velocity-strengthening model with a=0.0064, friction=0.52, long-term slip rate=75 mm/yr. The left plate shows horizontal displacements and the right one shows the vertical displacements. The red vector indicates the calculated result and the black one means the observation data. The fitness is not very good for this uniform rake afterslip model.

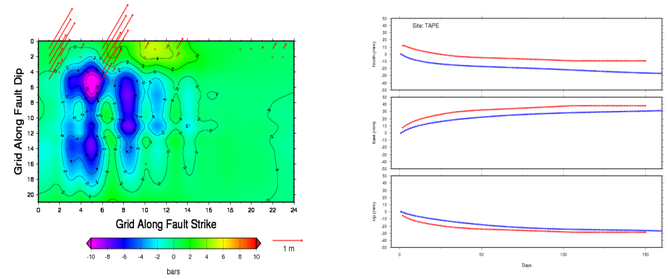

Most afterslips are central in the south of the fault plane shallower than 10 km and around the region with negative Coulomb failure stress changes due to the Chengkung earthquake. The afterslips creep with an uniform rake of 55 in degree shows an oblique thrust type behavior in Chihshang fault(Left plate). The right plate shows the best daily fitting at the TAPE continue GPS site. The daily evolution of displacement in three components is consistent with the observed direction but the magnitude. The blue and red lines indicate observed and calculated data, respectively.

6. References

Cheng, L.W., Lee, J.C., Hu, J.C. & Chen, H.Y., 2009. Coseismic and postseismic slip distribution of the 2003 Mw=6.5 Chengkung Earthquake in eastern Taiwan: elastic modeling from inversion of GPS data, *Tectonophysics*, **466**, 335-343, doi:10.1016/j.tecto.2007.11.021.

Ching, K.E., Rau, R.J. & Zeng Y. 2007. Coseismic source model of the 2003 M w 6.8 Chengkung earthquake, Taiwan, determined from GPS measurements, *J. Geophys. Res.*, **112**, B06422, doi:10.1029/2006JB004439.

Lee, J.C., Angelier, J., Chu, H.T., Hu, J.C., Jeng, F.S. & Rau, R.J., 2003. Active fault creep variations at Chihshang, Taiwan, revealed by creep meter monitoring, 1998–2001, *J. Geophys. Res.*, **108**, doi:10.1029/2003JB002394.

Lee, J.C., Chu, H.T., Angelier, J., Hu, J.C., Chen, H.Y. & Yu, S.B., 2006. Quantitative analysis of surface coseismic faulting and postseismic creep accompanying the 2003, Mw = 6.5, Chengkung earthquake in eastern Taiwan, *J. Geophys., Res.*, **111**, doi:10.1029/2005JB003612.

Perfettini, H. & Avouac, J.P., 2007. Modeling afterslip and aftershocks following the 1992 Landers earthquake, *J. Geophys. Res.*, **112**, doi:10.1029/2006JB004399.

Sambridge, M., 1999. Geophysical Inversion with a Neighbourhood Algorithm -I. Searching a parameter space, *Geophys. J. Int.*, **138** , 479-494.

Wu, Y.M., Chen, Y.G., Hu, J.C., Shin, T.C., Kuochen, H., Hou, C.S., Chang, C.H., Wu, C.F. & Teng, T.L., 2006. Coseismic versus interseismic ground deformations, fault rupture inversion and segmentation revealed by 2003 Mw 6.8 Chengkung earthquake in eastern Taiwan, *Geophys. Res. Lett.*, **33**, L02312, doi:10.1029/2005GL024711.